Available online at www.sciencedirect.com
ScienceDirect
Journal of Power Sources 177 (2008) 660–664
JOURNAL OF POWER SOURCES
www.elsevier.com/locate/jpowsour

Short communication

Investigation on capacity fading of aqueous $MnO_2{\cdot}nH_2O$ electrochemical capacitor

Yi-Chien Hsieh [a], Kuang-Tsin Lee [a], Yen-Po Lin [a], Nae-Lih Wu [a,*], Scott W. Donne [b]

[a] *Department of Chemical Engineering, National Taiwan University, Taipei 106, Taiwan*
[b] *Discipline of Chemistry, University of Newcastle, Callaghan, NSW 2308, Australia*

Received 25 May 2007; received in revised form 10 November 2007; accepted 12 November 2007
Available online 19 November 2007

Abstract

Cycle stability of $MnO_2{\cdot}nH_2O$ electrochemical capacitors (ECs) has been studied by using galvanostatic tests and electrochemical impedance spectroscopy (EIS). The extent of capacity fading, ranging from 5 to 30% in 1000 cycles, increases with current-rate, and is markedly reduced with increasing binder content. Two fading mechanisms have been identified. With low binder content, and at high current-rate, capacity fading occurs in conjunction with appreciable increase in transmission resistance, suggesting progressively deteriorating electric contacts among the pseudocapacitive oxide particles and conductive carbon. The mechanical failure of the electrode structure may arise from the cyclic volumetric variation of the pseudocapacitive oxide particles as previously reported. With high binder content or at low current-rate, capacity fading is associated with increasing interfacial charge-transfer resistance upon cycling, which has a less pronounced effect than the mechanical failure mechanism.

Keywords: Electrochemical capacitor; MnO_2; Cycle stability; Capacity fading

1. Introduction

Electrochemical capacitors (ECs) are promising energy storage devices for meeting the high-power electronic device market [1–3]. For practical applications, an EC must fulfill the requirement of long cycle life, typically more than tens of thousands of cycles, under high charge/discharge (C/D) current-rate conditions. Hydrated amorphous/nanocrystalline manganese oxide, $MnO_2{\cdot}nH_2O$ [4,5], has drawn much attention as a promising EC electrode material; it exhibits capacitances exceeding $200\,F\,g^{-1}$ in solutions of alkali salts [4–8] and has the advantages of low cost and environment-benign nature. There have been a few references touching upon the issue of cycling stability of $MnO_2{\cdot}nH_2O$ EC, but they presented controversial results. For instance, Toupin et al. [6] reported essentially no capacity loss after 1000 cycles for a thick-film (>100 μm) electrode in a cyclic voltammetry (CV) test under a slow potential scan rate of $2\,mV\,s^{-1}$. On the other hand, Anderson et al. [7,8] reported more than 10% capacity loss after 1500 cycles with a potential scan rate of $50\,mV\,s^{-1}$ for very thin (<15 $\mu g\,cm^{-2}$) $MnO_2{\cdot}nH_2O$ electrode prepared by a sol–gel process.

Anderson et al. attributed their observed capacity loss mainly to partial dissolution of the oxide film, probably by disproportionation reaction [7,8]. The same mechanism has also been quoted by Reddy and Reddy [9], who also observed more than 50% capacitance loss on their MnO_2 ambigel after 800 cycles. On the other hand, in our previous investigation [10] on the pseudocapacitance mechanism of $MnO_2{\cdot}nH_2O$, it was found by using in situ synchrotron X-ray diffraction that, upon cycling, the oxide phase experienced cyclic lattice expansion/contraction by ∼2.5% over a potential range of 1.0 V. The lattice expansion naturally leads to three-dimensional volumetric expansion/contraction of individual oxide particles, which could be detrimental to the stability of electrode structure.

In this paper, the cycle stability of conventional thick-film electrodes of $MnO_2{\cdot}nH_2O$ particles prepared by the slurry-coating technique and containing poly-vinylidene-fluoride (PVdF) as the binder constituent was systematically studied using constant-current cycling tests and electrochemical impedance spectroscopy (EIS) analysis. Experimental results indicate that mechanical failure of electrode structure can indeed

* Corresponding author. Tel.: +886 2 23627158; fax: +886 2 23623040.
E-mail addresses: nlw001@ntu.edu.tw, nlw001@ccms.ntu.edu.tw (N.-L. Wu).

0378-7753/$ – see front matter © 2007 Elsevier B.V. All rights reserved.
doi:10.1016/j.jpowsour.2007.11.026

be a serious issue in causing charge-storage capacity fading of $MnO_2{\cdot}nH_2O$ EC.

2. Experimental

$MnO_2{\cdot}nH_2O$ particles were precipitated by mixing 0.15 M $KMnO_4$ and 0.15 M $MnSO_4$ aqueous solutions with a Mn(VII)/Mn(II) molar ratio of 2:3 (stoichiometric) at 25 °C. After thoroughly washing with de-ionized water, the particles were finally heated at 200 °C for 1 h in air. To prepare the electrode, slurry containing the oxide powder, acetylene black (AB), and PVdF was coated onto Ti foils, and finally dried at 120 °C for 6 h in vacuum. On the dry basis, the oxide to AB ratio was fixed at 7:3, while the binder, which used *N*-methyl pyrrolidone (NMP, Mitsubishi Chemical) as the dispersing solvent, had a weight composition of either 7.2 or 13.4%. The electrodes and cells will hereafter be referred to with a prefix of 7 and 13%, respectively, to indicate their binder contents. Every electrode contains approximately 5.0 mg cm^{-2} of dried overlay materials, although the weight may vary slightly (±10%) from one electrode to another.

Electrochemical characterizations, including cyclic voltammetry, constant-current cycling, and EIS, were carried out with a symmetric two-electrode configuration, where two $MnO_2{\cdot}nH_2O$ electrodes of 1 cm × 1 cm were clamped between two glass slides and separated with a porous separator (BS0712, Coin Nano Tech), and the electrolyte is aqueous 1 M NaCl. The tests were carried out on an electrochemical analyzer (Eco Chemie PGSTAT30). Inductively coupled plasma (ICP) spectroscopy (Optima 3000XL) was employed to determine the Mn content in electrolyte solution.

3. Results and discussion

Fig. 1 summarizes the CV data at different scan rates for a typical $MnO_2{\cdot}nH_2O$ cell employed in the present study. The voltammograms exhibit essentially rectangular-shaped profiles, characteristic of a capacitor. By taking into account of the electrode overlay, composition, and subtracting the contribution from the carbon component (~10.0 F g^{-1} C), the specific capacitance of the oxide phase was calculated to be

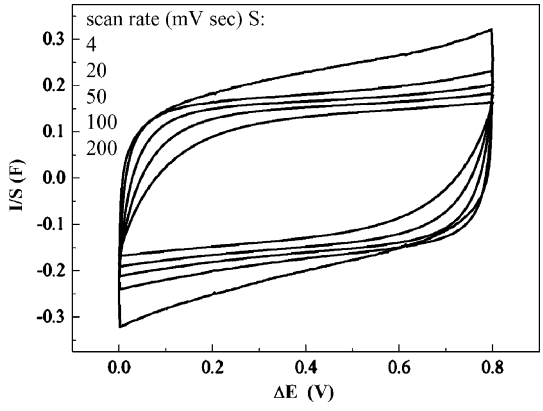

Fig. 1. Cyclic voltammograms of a symmetric $MnO_2{\cdot}nH_2O$ electrochemical capacitor (electrolyte: 1 M NaCl).

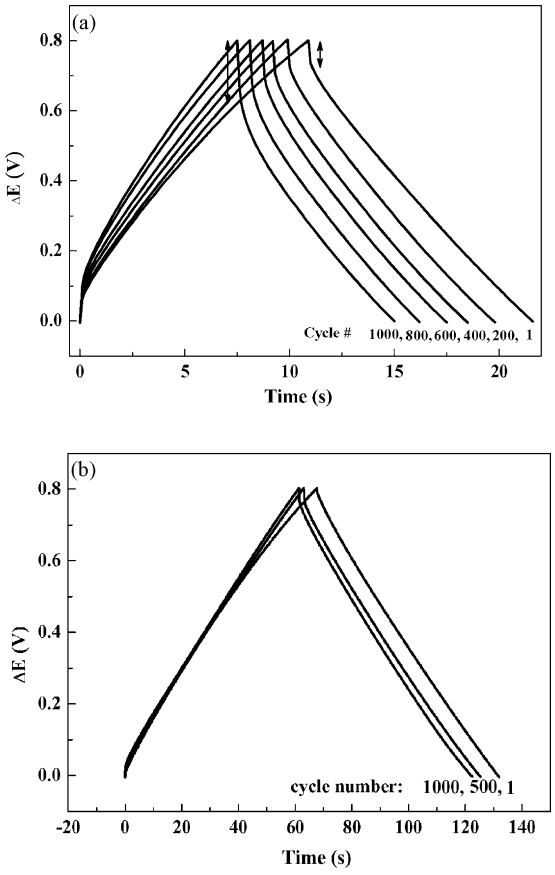

Fig. 2. Chrono-voltage plots of symmetric $MnO_2{\cdot}nH_2O$ electrochemical capacitors made with 7% binder under the current rate of (a) 2.0 A g^{-1} and (b) 0.5 A g^{-1}.

134.6 F g^{-1} $MnO_2{\cdot}nH_2O$. Higher specific capacitances exceeding 200 F g^{-1} of $MnO_2{\cdot}nH_2O$ have been reported in the literature [6,7] but only for much thinner electrodes.

The C/D cycling tests were carried out at current densities of 2.0 and 0.5 A g^{-1} (the current densities are based on the total weight of the active materials, including $MnO_2{\cdot}nH_2O$ and AB). A current density of 2.0 A g^{-1} corresponds approximately to a scan rate of ~60 mV s^{-1} in the CV test, and 0.5 A g^{-1} to ~15 mV s^{-1}. Fig. 2a shows the chrono-voltage curves of selected cycles carried out at 2.0 A g^{-1} for a typical cell of which the electrodes contain 7.2% binder (i.e., the 7% cell). From the charge branches of these curves, it is clear that the charge storage capacity (ΔQ) progressively decreases with increasing cycle number. The capacity was found to lose 29.4% of its initial value after 1000 cycles (Fig. 3). Concurrently, the IR drop was found to gradually increase with cycle number, suggesting continuously increasing resistance along the electron conduction pathways within the electrodes. The same trend has been observed for several cells from different batches, although there are small variations in the exact extents of fading. The symmetric cells were dissembled at the end of cycling, and the electrodes were then individually measured for their capacities with a three-electrode configuration. The results showed that the electrodes exhibited similar extents of fading and there was no regular pattern indicating either of the electrodes in a cell faded faster than the other.

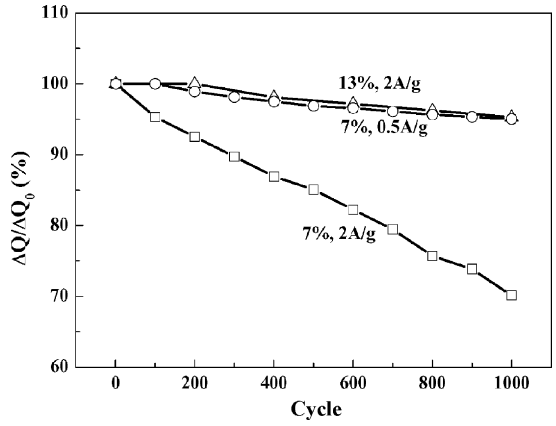

Fig. 3. Charge-storage retention ratio, $\Delta Q/\Delta Q_0$ vs. cycle number for the symmetric $MnO_2{\cdot}nH_2O$ electrochemical capacitors made with different binder contents (7 and 13 wt.%) and under different current rates.

Tests with 0.5 A g^{-1} show that the capacity fading rate was reduced as the current density decreased (Fig. 3). It is noted that a lower current density corresponds to a longer period for each cycle. That is, the extent of capacity fading does not increase with the length of test period but rather with increasing current rate. Finally, it was found that increasing the amount of binder to 13.4% dramatically reduces the fading rate (Fig. 3). Under 2.0 A g^{-1}, the 13% cell exhibits an extent of fading of merely 5.8%, in contrast to 29.4% for the 7% cell.

Conway [11] suggested that a pseudocapacitor can be described by the equivalent circuit shown in Fig. 4a. R_S is the solution resistance, and R_F corresponds to the charge-transfer resistance through the pseudocapacitance process. C_{dl} is the double-layer capacitance at the electrode/electrolyte interface, while C_P arises from the pseudocapacitance. This equivalent circuit gives a theoretical Nyquist plot consisting of a semi-circle at high-frequency region followed by a vertical line within the low-frequency region. The parallel R_F–C_{dl} configuration accounts for the semi-circle feature, while C_P for the steep line.

Fig. 5a shows the Nyquist plot of a fresh $MnO_2{\cdot}nH_2O$ cell. The plot shows a depressed semi-circle above ~240 Hz and a steep line below 2 Hz. They are largely consistent with the model. The deviations, including the depression in semi-circle

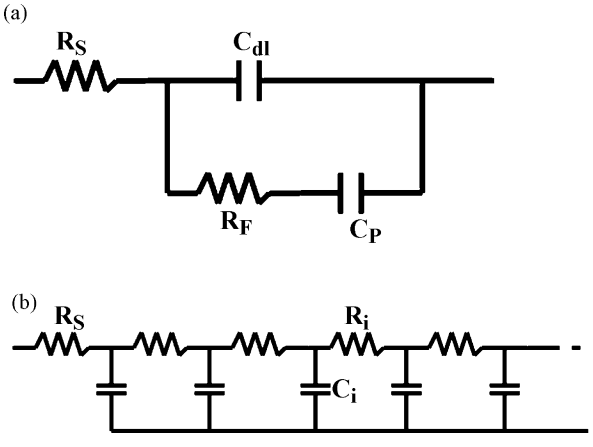

Fig. 4. Equivalent circuit for (a) pseudocapacitor and (b) transmission-model.

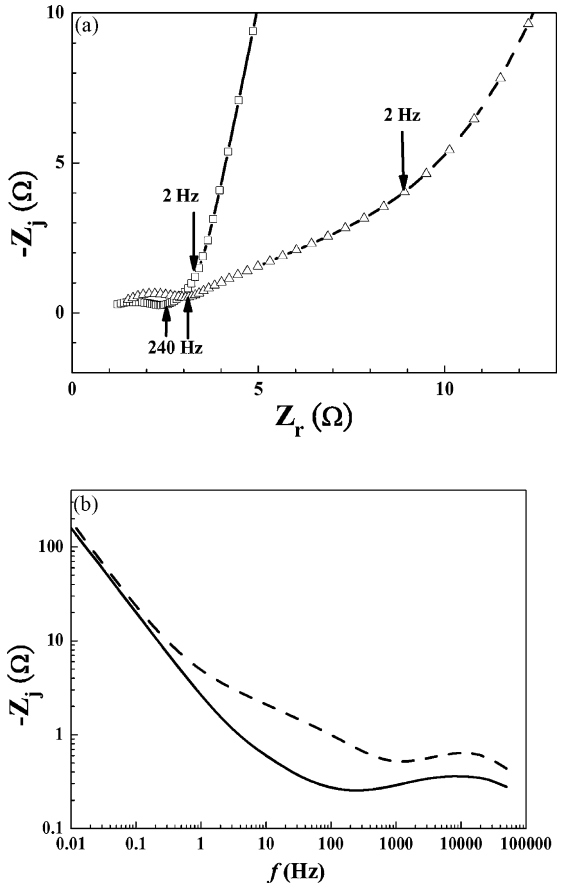

Fig. 5. AC impedance data for the symmetric $MnO_2{\cdot}nH_2O$ electrochemical capacitors made with 7% binder before (□, solid-line) and after (Δ, dashed-line) under the current rate of 2.0 A g^{-1}. (a) Nyquist plots: Z_r vs. $-Z_j$ (↓ locates 2 Hz and ↑ locates 240 Hz); (b) $-Z_j$ vs. f (frequency).

and line inclination, can be attributed to the porous nature of the electrode [12,13]. Additionally, there was noticed a short curved region between 2 and 240 Hz. This region is not predicted by the circuit model in Fig. 4a and will be discussed below, where it developed with cycling.

The logarithm plot of the imaginary part of the impedance versus frequency ($-Z'$ to f plot in Fig. 5b) shows a peak above ~200 Hz and an inclined line at lower frequencies. There exists one-to-one correspondence between Fig. 5a and b. The peak, indicative of a parallel RC element, corresponds to the semi-circle loop in the Nyquist plot. On the other hand, the inclined line within the low-frequency range corresponds to a capacitor.

After 1000 cycles at the rate of 2.0 A g^{-1}, the Nyquist plot (Fig. 5a) of the cycled cell shows a slight expanding in the high-frequency semi-circle and, more profoundly, an inclined line with an inclination angle of ~31° within the middle-frequency range (within 2–240 Hz), which shifts the capacitor (steep) line along the real axis to higher resistance. The overall resistance has been increased nearly threefold. In its $-Z'$ to f plot (Fig. 5b), there exists an additional broad hump between ~2.0 and 240 Hz. This mid-frequency inclined line in the Nyquist plot is believed to have similar nature as the short-curved region observed for the fresh sample within the same frequency range. These mid-frequency features may arise from the granular and porous nature

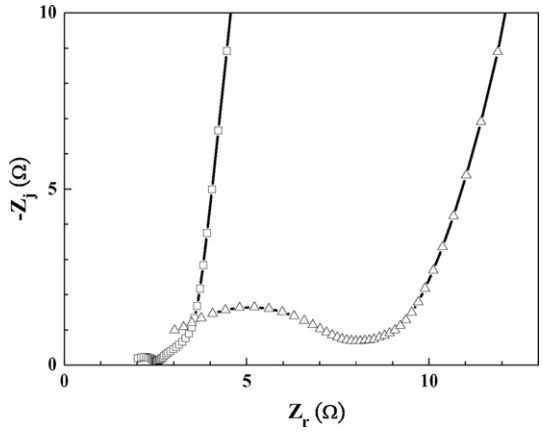

Fig. 6. Nyquist plots for the symmetric $MnO_2{\cdot}nH_2O$ electrochemical capacitors made with 7% binder before (□, solid-line) and after (Δ, dashed-line) under the current rate of 0.5 A g^{-1}.

of the electrode, and they can be accounted for by a transmission-line model that contains distributed *RC* network as schematically shown in Fig. 4b [11–13]. In the generalized sense of the model, the resistances (*R*) sum up the pore resistances and the electric resistances along the solid conductive matrix over different segments within an electrode. The electric resistance is determined to a greater extent by contact resistances between the grains than by the bulk resistances within the grains. For the *RC* network having infinite numbers of equal-valued *R*s and *C*s, the line has a theoretical inclination of 45°. On the other hand, it can readily be demonstrated that the angle deviates from the ideal value for varied *R*s and *C*s. The results shown in Fig. 5a and b indicates that the overall resistance of this distributed *RC* network increases more than eight times, from ∼0.7 to 5.8 Ω, after cycling at the current rate of 2.0 A g^{-1}.

On the other hand, Fig. 6 compares the Nyquist plots before and after cycling at 0.5 A g^{-1}. Compared with those at 2.0 A g^{-1} (Fig. 5a), two major differences can be noticed. The plots of the low current-rate show a large increase in the semi-circle resistance that is associated with the charge-transfer process (Fig. 4a) at the solid-electrolyte interface after cycling. In contrast, there is much less change in the transmission-model network resistance.

Capacity fading of $MnO_2{\cdot}nH_2O$ EC has mostly been attributed to dissolution of the oxide film into the electrolyte [7–9]. The electrolyte solutions of the 7% cells after cycling have been analyzed for Mn content by ICP analysis. As shown in Table 1, Mn dissolution has indeed been detected for either low- or high-rate condition, but the amount of dissolution has always been less than 0.5%. On the one hand, the amount of dissolution is too low to account for the extent of capacity fading in either case (Fig. 3). On the other hand, the cell which exhibits more capacity fading at the higher current-rate in fact shows smaller amount dissolution. These results may indicate that the dissolution mechanism cannot be a significant cause to the capacity fading in the present study. Indeed, it also fails to explain the remarkable effect of the binder content in suppressing the fading.

Table 1
Mn content in electrolytes for the 7% binder cells

Charge/discharge current rates (A g^{-1})	Measured Mn content in 15 mL (ppm)	Molar ratio of dissolved Mn–Mn in electrode (%)
0.5	0.48 (±2%)	0.44
2.0	0.21(±3%)	0.19

Our previous study [10] on the pseudocapacitance mechanism of $MnO_2{\cdot}nH_2O$ in aqueous alkali salts solutions has shown that the mechanism involves charge-transfer at Mn-ion sites balanced by bulk insertion/extraction of the solution cations into/from the oxide structure. The reaction can be expressed as:

$$\mathrm{Mn(IV)O_2{\cdot}}n\mathrm{H_2O} + \delta\mathrm{e}^- + \delta(1-f)\,\mathrm{H_3O}^+ + \delta f\, M^+ \leftrightarrow (\mathrm{H_3O})_{\delta(1-f)}M_{\delta f}[\mathrm{Mn(III)}_\delta\mathrm{Mn(IV)}_{1-\delta}]\mathrm{O_2{\cdot}}n\mathrm{H_2O},$$

where M^+ is alkali cation. In the case of aqueous NaCl electrolyte, f is nearly zero. In situ synchrotron X-ray diffraction study showed reversible lattice expansion/contraction (∼2.5% over 1.0 V) of $MnO_2{\cdot}nH_2O$ crystallites upon cycling [10]. Cyclic dimensional variation of the active components within an electrode has long been known to have significant impact on the stability of electrode structure upon cycling. The present data indeed give strong support to the notion of mechanical failure of electrode structure arising from such dimensional variations. The effect of cyclic volumetric expansion/contraction of the oxide particles on the electrode structure can be envisioned as follows. During the expansion phase of a cycle, the particles, either oxide or C, are pushing one another, leading to extensive relative motion among particles, accompanied with macroscopic expansion of the entire electrode overlay. The binder connecting between the particles is simultaneously stretched in response to the particle motion. During the contraction phase, the particles tend to move back to the original positions, and the binder is relaxed. Upon cyclic stretching/relaxation, the binder may gradually become ruptured, fatigued, or mostly likely de-bonded with the particles, causing the electrode structure to become loose and the particles to lose electric contact between one another. A direct consequence will be increasingly deteriorating electric contacts between particles, leading to capacity reduction and increased *RC* network resistance.

Dahn et al. [14] once tested the mechanical properties of a PVDF (20 wt.%)-bound carbon black electrode, and showed a macroscopic elongation at break of ∼4.5% for the electrode at the strain rate of 1% min^{-1}. Given that the present electrodes contained merely one-third of the amount of PVDF (7 wt.%), it is reasonable to anticipate mechanical failure to occur with a macroscopic elongation far less than 4.5%.

The mechanical failure mechanism is also consistent with other observations. A higher current-rate introduces a greater strain rate and/or non-homogeneity in stress distribution, resulting in a greater extent of destruction. This may explain the observation that capacity fading increases with increasing C/D current-rate. On the other hand, using a greater amount of binder strengthens the overall binding between particles, and hence effectively suppresses capacity fading as observed (Fig. 3). Furthermore, the deteriorating electric contacts between particles can introduce pronounced distributed *RC* network equivalently

describing the poor particle–particle contacts. This explains the characteristics of *RC* network in the Nyquist plot after cycling (Fig. 5b). Finally, the mechanism may also explain why Anderson et al. [7,8] detected greater capacity fading than Toupin et al. [6] as described in Section 1. The former employed a scan rate of 50 mV s^{-1}, while the latter 2 mV s^{-1}.

It is also of interest to understand potential cause(s) to capacity fading at low current-rate. As shown in Figs. 5a and 6, both the 2.0 and 0.5 A g^{-1} cells show increase in charge-transfer resistance after cycling, although the latter shows a far more pronounced effect. The results indicate progressive modification in the oxide/electrolyte interfacial properties during cycling, and that tends to gradually impose additional resistance to the interfacial charge-transfer process. Furthermore, the extent of the modification seems to increase with reduced current-rate. In previous work by Donne [15] it has been shown that birnessite phase MnO_2 tends to be irreversibly reduced to Mn_3O_4 under deep discharge at slow cyclic scanning rate (0.02 mV s^{-1}), and Mn_3O_4 is electrochemically inactive. Given the similar synthesis procedures used in this work, and hence the anticipated similar manganese dioxide structure, an identical reaction might have taken place at the oxide surfaces in the present case, accounting predominantly for the capacity fading under 0.5 A g^{-1} and partially under 2 A g^{-1}.

In summary, the cycle stability of $MnO_2{\cdot}nH_2O$ EC has been studied by galvanostatic tests with different rates and impedance analysis on electrodes having different binder compositions. Experimental results show that the capacity fading of the EC increases dramatically with increasing current-rate. The accelerated fading can be attributed to gradual mechanical failure of the electrode structure during cycling. The failure causes increasingly deteriorating electric contacts among the constituent particles within the electrode, and it is believed to arise from cyclic volumetric variations of the oxide particles upon cycling. In addition, increasing interfacial charge-transfer resistance upon cycling has been found to play an important role in capacity fading at low current-rate.

Acknowledgments

This work is supported by the National Science Council of Taiwan, ROC (NSC 95-2221-E-002-350-MY3) and by National Taiwan University (95R0066-BE04-01).

References

[1] B.E. Conway, J. Electrochem. Soc. 138 (1991) 1539.
[2] B.E. Conway, V. Briss, J. Wojtowicz, J. Power Sources 66 (1997) 1.
[3] S. Sarangapani, B.V. Tilak, C.-P. Chen, J. Electrochem. Soc. 143 (1996) 3791.
[4] H.Y. Lee, J.B. Goodenough, J. Solid State Chem. 144 (1999) 220.
[5] H.Y. Lee, V. Manivannan, J.B. Goodenough, C.R. Acad. Sci. Paris, t. 2, série II c (1999) 565.
[6] M. Toupin, T. Brousse, D. Bélanger, Chem. Mater. 14 (2002) 3946.
[7] S.C. Pang, M.A. Anderson, T.W. Chapman, J. Electrochem. Soc. 147 (2000) 444.
[8] S.C. Pan, M. Anderson, J. Mater. Res. 15 (2000) 2096.
[9] R.N. Reddy, R.G. Reddy, J. Power Sources 124 (2003) 330.
[10] L. Kuo, N.L. Wu, J. Electrochem. Soc. 153 (2006) A1317.
[11] B.E. Conway, Electrochemical Supercapacitors: Scientific Fundamentals and Technological Applications, vol. 384, Plenum, New York, 1999, p. 544.
[12] R. de Levie, Electrochim. Acta 8 (1963) 751.
[13] C. Porter, P.L. Taberna, P. Simon, C. Laberty-Robert, Electrochim. Acta 49 (2004) 905.
[14] Z. Chen, L. Christensen, J.R. Dahn, J. Electrochem. Soc. 150 (2003) A1073.
[15] S.W. Donne, PhD Thesis, University of Newcastle, 1996.